

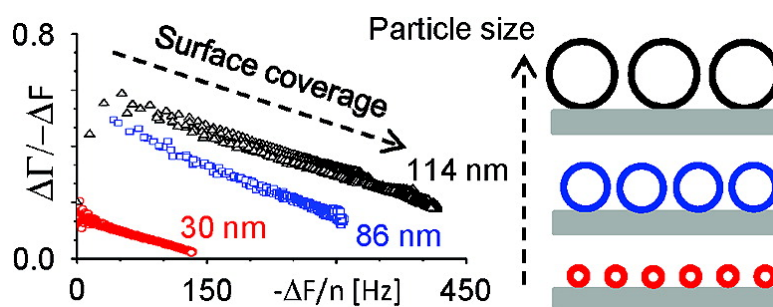
Article

Model-Independent Analysis of QCM Data on Colloidal Particle Adsorption

Eduarne Tellechea, Diethelm Johannsmann, Nicole F. Steinmetz, Ralf P. Richter, and Ilya Reviakine

Langmuir, Article ASAP • DOI: 10.1021/la803912p • Publication Date (Web): 24 March 2009

Downloaded from <http://pubs.acs.org> on March 26, 2009



More About This Article

Additional resources and features associated with this article are available within the HTML version:

- Supporting Information
- Access to high resolution figures
- Links to articles and content related to this article
- Copyright permission to reproduce figures and/or text from this article

[View the Full Text HTML](#)

Model-Independent Analysis of QCM Data on Colloidal Particle Adsorption

Edurne Tellechea,[†] Diethelm Johannsmann,[‡] Nicole F. Steinmetz,[§] Ralf P. Richter,^{†,||} and Ilya Reviakine^{*,†}

[†]Centro de Investigación Cooperativa en Biomateriales, Parque Tecnológico de San Sebastián, E-20009 San Sebastián, Spain, [‡]Institute of Physical Chemistry, Clausthal University of Technology, Clausthal-Zellerfeld, D38678, Germany, [§]Department of Cell Biology, Center of Integrative Molecular Biosciences, The Scripps Research Institute, La Jolla, California 92037, and ^{||}Biosurfaces Unit, CIC biomaGUNE, Paseo Miramon 182, 20009 Donostia – San Sebastian, Spain, and Department of New Materials and Biosystems, Max-Planck-Institute for Metals Research, Heisenbergstrasse 3, 70569 Stuttgart, Germany

Received November 26, 2008. Revised Manuscript Received January 19, 2009

Quartz crystal microbalance (QCM) is widely used for studying soft interfaces in liquid environment. Many of these interfaces are heterogeneous in nature, in the sense that they are composed of discrete, isolated entities adsorbed at a surface. When characterizing such interfaces, one is interested in determining parameters such as surface coverage and size of the surface-adsorbed entities. The current strategy is to obtain this information by fitting QCM data—shifts in resonance frequency, ΔF , and bandwidth, $\Delta\Gamma$ —with the model derived for smooth, homogeneous films using the film acoustic thickness and shear elastic moduli as fitting parameters. Investigating adsorption of liposomes and icosahedral virus particles on inorganic surfaces of titania and gold, we demonstrate that the predictions of this model are at variance with the experimental observations. In particular, while the model predicts that the ratio between the bandwidth and frequency shifts, $\Delta\Gamma/\Delta F$ (the D/f ratio), should increase with both surface coverage and particle size, we observe that this ratio *increases* with increasing particle size but *decreases* with increasing surface coverage, demonstrating that QCM response in heterogeneous films, such as those composed of adsorbed colloidal particles, does not conform with the predictions of the homogeneous film model. Employing finite element method (FEM) calculations, we show that hydrodynamic effects are the cause of this discrepancy. Finally, we find that the size of the adsorbed colloidal particles can be recovered from a model-independent analysis of the plot of the $\Delta\Gamma/\Delta F$ ratio versus the frequency shift on many overtones.

Introduction

Interfaces between biological systems and nonbiological materials arise in the context of material biocompatibility, biosensor and biomaterial development, and basic biophysical studies that rely on the plethora of surface sensitive techniques for studying biological phenomena.^{1,2} Such interfaces are typically strongly hydrated and rather poorly defined, in the sense that they consist of either isolated, frequently polydisperse, objects (e.g., surface-adsorbed proteins or liposomes) or some diffuse continuous layers (polymer brushes, hydrogels). Poor density contrast between the bulk water and the strongly hydrated interface makes investigation of such interfaces with most (e.g., optical) techniques difficult. Here, acoustic techniques such as quartz crystal microbalance (abbreviated QCM^{3–6} or QCM-D^{7–9}) have an

advantage: acoustically, there is a significant difference between bulk water and a layer of organic material.^{5,10}

QCM is based on a thin quartz crystal oscillating in a shear–thickness mode at its resonance frequency.³ In a typical experiment, changes in resonance frequency, ΔF , and in half-width at half-maximum (“bandwidth” for short), $\Delta\Gamma$, relative to those of a bare crystal in liquid, are monitored on several overtones as a film is allowed to form at the surface of the crystal. An equivalent measure of bandwidth is dissipation, D , related to the latter as $D = 2\Gamma/f$, with f being the resonance frequency. In the case of thin, homogeneous films, these changes in frequency and bandwidth are related to the thickness and elastic properties of the film^{5,6} according to a well-established model based on the propagation of shear waves in viscoelastic media:

$$\Delta F^* = \Delta F + i\Delta\Gamma = -\frac{2f^2}{nZ_q} h_f \rho_f \left(1 - \frac{J_f^* i\omega\eta_{\text{liq}}\rho_{\text{liq}}}{\rho_f} \right) \quad (1)$$

where the asterisk denotes complex quantities, ΔF and $\Delta\Gamma$ are frequency and bandwidth shifts, respectively, $f = \omega/(2\pi)$ is the resonance frequency, n is the overtone order, Z_q is the acoustic impedance of quartz, h , ρ , η , and J^* are the acoustic thickness, density, viscosity, and complex shear compliance, respectively, and subscripts q, f, and liq refer to quartz, film, and liquid, respectively. The shear compliance, J^* , is the complex

*Correspondence should be addressed to I.R. at ireviakine@cicbiomagune.es.

- (1) Kasemo, B. *Surf. Sci.* **2002**, *500*(1–3), 656–677.
- (2) Tirrell, M.; Kokkoli, E.; Biesalski, M. *Surf. Sci.* **2002**, *500*(1–3), 61–83.
- (3) Cady, W. G. *Piezoelectricity*; McGraw-Hill Book Company, Inc.: New York, **1946**.
- (4) Ward, M. D.; Buttry, D. A. *Science* **1990**, *249*(4972), 1000–1007.
- (5) Johannsmann, D. Studies of Viscoelasticity with the QCM. In *Piezoelectric Sensors*, 1st ed.; Steinem, C., Janshoff, A., Eds.; Springer: New York, **2006**; pp 49–110.
- (6) Sauerbrey, G. *Z. Phys.* **1959**, *155*, 206–222.
- (7) Rodahl, M.; Hook, F.; Fredriksson, C.; Keller, C.A.; Krozer, A.; Brzezinski, P.; Voinova, M.; Kasemo, B. *Faraday Discuss.* **1997**, *107*, 229–246.
- (8) Rodahl, M.; Hook, F.; Krozer, A.; Brzezinski, P.; Kasemo, B. *Rev. Sci. Instrum.* **1995**, *66*(7), 3924–3930.
- (9) Rodahl, M.; Hook, F.; Kasemo, B. *Anal. Chem.* **1996**, *68*(13), 2219–2227.
- (10) Reimhult, E.; Larsson, C.; Kasemo, B.; Hook, F. *Anal. Chem.* **2004**, *76*(24), 7211–7220.

inverse of the shear modulus, G^* . Equation 1 holds in the thin film limit. Although not immediately apparent, one needs at least five parameters to perform full-fledged fits of experimental data with eq 1: film thickness, h_f , the real and the imaginary parts of the compliance at some reference frequency $J'(f_{\text{ref}})$ and $J''(f_{\text{ref}})$, and two more parameters describing the dependence of J on frequency. For details, see refs 5 and 11. This raises the question of whether there is a well-defined way to analyze experimental QCM data without resorting to fitting. For thin films, precise statements can be formulated if the ratio of the bandwidth shift to the frequency shift (the Df ratio) is examined instead of the shifts themselves. This ratio was first discussed by Krim and Widom in the context of nanotribology;¹² the authors used the Df ratio to derive a momentum relaxation time (a slip time) of noble gas atoms adsorbed to the electrode surface. In the context of adsorption from the liquid phase, the interpretation of the Df ratio is different. One has

$$\frac{\Delta\Gamma}{-\Delta F} \approx 2\pi f \eta_{\text{liq}} J_f' + 2\pi f h_f \sqrt{\rho_{\text{liq}} \pi f \eta_{\text{liq}}} (J_f' + J_f'') = \omega \eta_{\text{liq}} \left(J_f' + \frac{h_f}{\delta} (J_f' + J_f'') \right) \quad (2)$$

$\delta = (2\eta_{\text{liq}}/(\rho_{\text{liq}}\omega))^{1/2}$ is the (real) penetration depth of the shear wave. It was previously shown by Du et al. that, in the limit of very thin films, only the first term is relevant and the ratio is independent of the film thickness; it then is a materials parameter. Similarly, Tsortos et al.¹³ recently found the $\Delta\Gamma/-\Delta F$ ratio to be independent of the surface coverage in the case of surface-grafted DNA molecules. They showed that it was instead related to the intrinsic viscosity of the layer. The latter is essentially a materials parameter, which for polymers depends on the shape and molecular weight of the chains. The authors use this information to distinguish the shape and size of the surface-anchored DNA molecules.¹³ The effect of film thickness does appear in the higher-order term; the derivation of eq 2 is presented in the Appendix.

When investigating heterogeneous films, consisting of individual entities—such as liposomes, protein molecules, or virus particles adsorbed at a solid surface—one is interested in determining the surface coverage θ and the size of individual entities (defined in Figure 1), the dependence of these two parameters on various environmental factors (e.g., their size and concentration in solution, type of surface, pH, and so on), and interfacial mechanical properties. Acoustic thickness and shear elastic constants of such heterogeneous films have been determined from the fits of QCM data with eq 1, where the film is assumed to be homogeneous.^{10,14–18} One treats the sample within the framework of an effective medium theory. The derived fit parameters pertain to an “equivalent

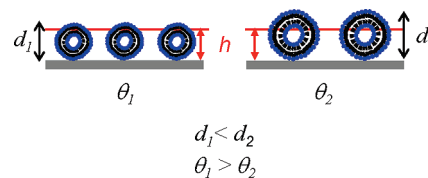


Figure 1. Acoustic thickness, h , measured by QCM is related to the size of the objects (height of the adsorbed liposomes, d) as well as their surface coverage θ (their number per unit area). Different combinations of d and θ may therefore result in the same acoustic thicknesses. The unknown contribution of the surrounding liquid to the acoustic thickness makes it difficult to separate the contributions of size and coverage to the frequency and bandwidth shifts.

homogeneous layer”. However, in the case of measurements performed in liquids on spatially separated objects, there is no simple relationship between this acoustic thickness and the compliance, on the one hand, and object size and surface coverage, on the other. In particular, we have recently shown that, for surface-adsorbed proteins, the relationship between the frequency shift and the surface coverage is not linear and the shear compliance, J_f^* , obtained from the fit of the QCM data with eq 1, contains surface coverage-dependent hydrodynamic contribution.^{19,20} On a phenomenological level, a recently proposed model that assigns a solvation coat of a defined shape and size to each adsorbed particle and accounts for the random distribution of particles on the surface was also found to reproduce the relative contribution of the solvent to the QCM frequency response very well.²¹

In this study, we use the adsorption of two types of colloidal particles on inorganic surfaces to investigate the QCM response at heterogeneous interfaces: ~ 30 nm icosahedral cowpea mosaic virus (CPMV) particles and extruded dipalmitoyl phosphatidyl choline (DPPC) liposomes of two sizes (~ 80 and ~ 120 nm). These three sets of particles provide a robust model system for the purposes of this study because of the well-defined sizes, spherical morphology, and stiffness (in the sense that they are not expected to significantly deform upon adsorption; some information concerning deformation of proteins upon adsorption and stiffness of virus particles can be found in refs 20 and 22–24).

We show that the contributions of size and surface coverage to the acoustic thickness (Figure 1) can be separated from each other by examining the behavior of the $\Delta\Gamma/-\Delta F$ ratio: it increases with particle size but decreases with surface coverage. This latter observation is at variance with predictions of the model based on homogeneous layers (eq 2); we use finite element method calculations to show that hydrodynamic effects are at the root of the discrepancy. Interestingly, the decrease of the $\Delta\Gamma/-\Delta F$ ratio is linear in ΔF over a large range of ΔF . We find that this linear dependence may be used to estimate the size of the adsorbed objects without fitting the data with a model.

- (11) Johannsmann, D. *Phys. Chem. Chem. Phys.* **2008**, *10*, 4516.
- (12) Krim, J.; Widom, A. *Phys. Rev. B* **1988**, *38*(17), 12184–12189.
- (13) Tsortos, A.; Papadakis, G.; Mitsakakis, K.; Melzak, K. A.; Gizeli, E. *Biophys. J.* **2008**, *94*(7), 2706–2715.
- (14) Larsson, C.; Rodahl, M.; Hook, F. *Anal. Chem.* **2003**, *75*(19), 5080–5087.
- (15) Hook, F.; Kasemo, B.; Nylander, T.; Fant, C.; Sott, K.; Elwing, H. *Anal. Chem.* **2001**, *73*(24), 5796–5804.
- (16) Patel, A. R.; Frank, C. W. *Langmuir* **2006**, *22*(18), 7587–7599.
- (17) Reviakine, I.; Rossetti, F. F.; Morozov, A. N.; Textor, M. *J. Chem. Phys.* **2005**, *122*(20), 204711–204718.
- (18) Hook, F.; Voros, J.; Rodahl, M.; Kurrat, R.; Boni, P.; Ramsden, J. J.; Textor, M.; Spencer, N. D.; Tengvall, P.; Gold, J.; Kasemo, B. *Colloids Surf., B* **2002**, *24*(2), 155–170.

- (19) Rojas, E.; Gallego, M.; Reviakine, I. *Anal. Chem.* **2008**, *80*(23), 8982–8990.
- (20) Johannsmann, D.; Reviakine, I.; Rojas, E.; Gallego, M. *Anal. Chem.* **2008**, *80*(23), 8891–8899.
- (21) Bingen, P.; Wang, G.; Steinmetz, N. F.; Rodahl, M.; Richter, R. P. *Anal. Chem.* **2008**, *80*(23), 8880–8890.
- (22) Liashkovich, I.; Hafezi, W.; Kuhn, J. E.; Oberleithner, H.; Kramer, A.; Shahin, V. *J. Cell Sci.* **2008**, *121*(14), 2287–2292.
- (23) Kol, N.; Shi, Y.; Tsvitov, M.; Barlam, D.; Shneck, R. Z.; Kay, M. S.; Rouso, I. *Biophys. J.* **2007**, *92*(5), 1777–1783.
- (24) Müller, D. J.; Engel, A. *Biophys. J.* **1997**, *73*(3), 1633–1644.

Materials and Methods

Materials. Dipalmitoyl phosphatidyl choline (DPPC) was purchased from Avanti Polar Lipids, Inc. (Alabaster, Alabama) in powder form and stored at $-20\text{ }^{\circ}\text{C}$ until used. Lipid stock solutions were prepared by dissolving the lipids in chloroform (Sigma-Aldrich, Madrid, Spain) and stored at $-20\text{ }^{\circ}\text{C}$ for no longer than two months. Lipid concentrations in the stock solutions were routinely tested by measuring the total phosphorus contents of the solutions using the procedure that can be found on the Avanti Polar Lipids Web site.

Cowpea mosaic virus (CPMV) was prepared as described previously.²⁵ A biotin-conjugated form of the virus nanoparticles was used, although this functionality was not exploited in this study.

The buffer used with the liposomes contained 10 mM HEPES, 150 mM NaCl, and 2 mM CaCl_2 , adjusted to pH 7.4 with NaOH. The buffer was filtered through sterile 200 nm pore diameter filters and degassed prior to use in each experiment. The buffer used with the CPMV additionally contained 3 mM NaN_3 .

Water used throughout this study was purified by a NANO-pure Diamond purification system from Barnstead. Chemicals were purchased from Sigma Aldrich (Madrid, Spain) or Scharlab (Barcelona, Spain).

Methods. Liposome Preparation and Characterization. Unilamellar liposomes were prepared by extrusion with a handheld LipoFast extruder from Avestin Inc., (Ottawa, Canada) essentially as described previously.^{26,27} Polycarbonate membranes with two pore sizes, 50 and 100 nm, were used. Extrusion was performed at $60\text{ }^{\circ}\text{C}$, above the main transition temperature of DPPC. Vesicle solutions were stored under argon at $4\text{ }^{\circ}\text{C}$ until used, but not longer than two weeks.

Liposome size was measured by dynamic light scattering with a Malvern Zetasizer Nano series instrument (Worcestershire, U.K.). The results of these measurements are presented in Table 1.

Quartz Crystal Microbalance (QCM) Measurements. QCM measurements using liposomes were performed with TiO_2 -coated quartz crystals from Q-Sense AB (Västra Frölunda, Sweden). Before each measurement, crystals were cleaned in a 2% (w/v) sodium dodecyl sulfate (SDS) solution for 30 min, rinsed under a stream of running ultrapure water, blow-dried with nitrogen gas, and treated in a UV/ozone cleaner (Bioforce Nanoscience, Ames, AL, U.S.A.) for 30 min. The UV/ozone cleaner was preheated for 30 min before the treatment. Measurements with CPMV were performed on Au-coated quartz crystals from Q-Sense AB. They were also UV/ozone treated for 30 min before use.

The measurements using liposomes were performed with a hybrid QCM system based on the E5100A network analyzer (Agilent, Spain) simultaneously connected to two flow modules (model 401, Q-Sense AB via ZFDC-20-3 + directional couplers (Minicircuits, Surrey, U.K.). The analyzer was controlled by a personal computer running the QTZ software (Resonant Probes GmbH, Goslar, Germany). Temperature was controlled with a water circulator, Analog model 912 from Polyscience (Illinois, U.S.A.). The experiments were performed at $20\text{--}21\text{ }^{\circ}\text{C}$.

QCM flow modules were cleaned before each experiment by sonicating them in Cobs Integra cleaner (Roche, Switzerland) for 30 min at $30\text{ }^{\circ}\text{C}$, and then in three changes of water for a total of 30 more minutes.

A clean crystal was mounted in the freshly cleaned flow cell and tested for oscillations at frequencies between 15 and 95 MHz ($n = 3\text{--}19$). In most of the experiments reported, all of

these overtones were found; in some, the two highest overtones could not be observed.

If at least six of the overtones were found, the cells were filled with buffer and data collected for a minimum of 30 min, to obtain a baseline in liquid. Several consecutive injections of buffer were performed to test the stability of the baseline.

After obtaining a stable baseline, 1 mL of 0.1 mg/mL temperature-equilibrated liposome suspension was injected into the measurement chamber. We are aware of the fact that the volume of these Q-Sense flow modules is exceedingly small, and therefore, flow-through measurements are preferred. However, to simplify the experimental protocol, we chose to use relatively large liposome concentrations and injection volumes; the choice of this procedure did not affect our results. After the liposome adsorption was complete, excess of nonadsorbed liposomes was removed by rinsing the surface with 1 mL of buffer.

Measurements on the deposition of CPMV were performed with the Q-Sense E4 system (Q-Sense AB), equipped with flow modules. The system was operated in flow mode, i.e., sample solution was continuously delivered to the measurement chamber by a multisyringe pump (KD Scientific, U.S.A.), using a flow rate of $20\text{ }\mu\text{L}/\text{min}$. In order to switch between sample liquids, the flow was interrupted for a few seconds without disturbing the measured signals. The working temperature was $23\text{ }^{\circ}\text{C}$. Shifts in frequency and dissipation were recorded for all resonances up to $n = 13$. CPMV particles were injected at a concentration of $20\text{ }\mu\text{g}/\text{mL}$.

Modeling

The calculation of the complex frequency shift, ΔF^* , builds on the small-load approximation, which states that ΔF is proportional to the stress–speed ratio at the crystal surface.^{28,29}

$$\frac{\Delta F^*}{f_F} \approx \frac{i}{\pi} \frac{Z_L}{Z_q} = \frac{i}{\pi Z_q} \frac{\sigma}{\dot{u}} \quad (3)$$

Here, $\Delta F^* = \Delta F + i\Delta\Gamma$ is the complex frequency shift, f_F is the frequency of the fundamental, $Z_q = 8.8 \times 10^6\text{ kg m}^{-2}\text{ s}^{-1}$ is the acoustic impedance of AT-cut quartz, $Z_L = \sigma/\dot{u}$ is the load impedance, σ is the stress, and \dot{u} is the lateral speed at the resonator surface; the two quantities have a phase relative to each other, and therefore, their ratio is a complex quantity. In the case of the purely inertial loading (adsorbed mass), this equation leads transparently to the Sauerbrey relationship, while for homogeneous viscoelastic layers it leads to eq 1. This is discussed in detail in refs 5 and 11, and these arguments will not be repeated here except to state that, since the frequency shift depends linearly on stress, the small-load approximation holds in an average sense. Therefore, for heterogeneous samples, one may insert the *area-average* of the stress distribution into eq 3. The calculation of the frequency shift then entails the calculation of the forces (stresses) acting on the surface of the crystal. In this study, this is achieved by means of the finite element method (FEM), which is used to calculate the forces generated by the liquid flowing around the surface-adsorbed objects of a particular geometry. The details of the modeling are reported in ref 20 but will be briefly summarized here for the sake of clarity and completeness.

FEM calculations were performed using the Multiphysics Module of the COMSOL software package (COMSOL

(25) Steinmetz, N. F.; Bock, E.; Richter, R. P.; Spatz, J. P.; Lomonosoff, G. P.; Evans, D. J. *Biomacromolecules* **2008**, *9*(2), 456–462.

(26) Reviakine, I.; Brisson, A. *Langmuir* **2000**, *16*(4), 1806–1815.

(27) Macdonald, R. C.; Macdonald, R. I.; Menco, B. P. M.; Takeshita, K.; Subbarao, N. K.; Hu, L. R. *Biochim. Biophys. Acta* **1991**, *1061*(2), 297–303.

(28) Johannsmann, D.; Mathauer, K.; Wegner, G.; Knoll, W. *Phys. Rev. B* **1992**, *46*(12), 7808–7815.

(29) Eggers, F.; Funck, T. *J. Phys. E: Sci. Instrum.* **1987**, *20*(5), 523–530.

Table 1

material	particle diameter (nm) ^a	$-\Delta F/n$ (Hz) ^b	Sauerbrey height (nm) ^d	ratio ^e
CPMV	28	175 ± 5	29 ± 0.8	1 ± 0.03
liposomes	83 ± 4	448 ± 32	81 ± 6	0.9 ₈ ± 0.1
	114 ± 8	616 ± 61	111 ± 11	0.9 ₇ ± 0.2
	1.4 ± 0.2 ^c	1.4 ± 0.2 ^c		

^aIn the case of liposomes, Z-averaged diameter measured by dynamic light scattering is shown. Average ± standard deviation was calculated from eight measurements. For CPMV, the averaged diameter based on the crystal structure is given;³⁰ the diameter of CPMV particles was also measured by light scattering. The result was found to correspond with the crystallographic dimensions (not shown). ^bExtrapolated frequency shifts, determined from the x-intercept of the $\Delta\Gamma/-\Delta F$ vs $-\Delta F/n$ plot. ^cRatio of liposome diameters and extrapolated frequency shifts. ^dExtrapolated Sauerbrey mass was calculated from the extrapolated frequency shifts using the Sauerbrey constant of 18 ng/(cm² Hz); the corresponding extrapolated Sauerbrey height is the mass divided by the density of the layer, 1.0 g/cm³ in the case of the liposomes and 1.08 g/cm³ in the case of the virus particles.²⁵ ^eThe ratio of the Sauerbrey height to the particle diameter in solution.

GmbH, Göttingen, Germany). Adsorbed colloidal particles were represented as hemispheres with the diameter of 114 nm, density of $\rho = 1.0$ g/cm³, and complex viscosity of $\eta = \eta' - i\eta''$, such that $|\eta| = 5$ mPa·s and $\tan(\delta) = \eta''/\eta' = 1.38$. The viscosity of the ambient liquid was 1 mPa·s, and its density was $\rho = 1.0$ g/cm³.

Cell geometry and mesh used in the calculations are shown in Figure 4a. Along the surface normal, the cell was 2 μ m long, which amounts to 8 times the penetration depth of the acoustic shear wave at 5 MHz. The penetration depth, δ , is 252 nm at this frequency.

Along the crystal surface (top of the cell), the width of the cell was varied to simulate the variation in the surface coverage that occurs during the adsorption process. “Surface coverage” was defined as the ratio of 114 nm (the diameter of adsorbed hemispheres) to the width of the cell. Neutral boundary conditions were applied at the domain boundaries on the bottom, the right, and the left. The domain boundary at the top side oscillated with an amplitude of $u_0 = 10^{-2}$ nm. More technically, the boundary was assigned a fixed “velocity”, where the velocity was defined as $i\omega u_0$. With regard to the mesh size, the default settings were modified in one respect, which was the maximum mesh size at the three-phase line (or, in 2D, the three-phase point) between the water, the adsorbate, and the wall. This was set to 0.001 nm (cf. Figure 4a). At this point, the simulation does not employ adaptive meshing, that is, the domain boundaries do not move with the fluid. As proven in the Supporting Information to ref 20, the error introduced by the fixed subdomain boundaries converges to zero in the limit of small amplitudes. Periodic boundaries were applied at the left and the right. The geometry therefore corresponds to an array of hemispheres.

Our computational resources only allowed for 2D FEM calculations. 3D modeling is possible, in principle, but one cannot afford the appropriate mesh size on a personal computer. In two dimensions, a hemisphere turns into a hemicylinder. Two calculations were therefore performed: one with the direction of flow parallel to the cylinders and one with the direction of flow perpendicular. When making the comparison with experiments, we applied arithmetic averaging over the two flow directions to both ΔF and $\Delta\Gamma$.

For cylinders aligned perpendicular to the direction of shear, we employed the 2D steady-state incompressible Navier–Stokes model. The model readily produces oscillating shear waves if the term $-i\omega\rho v$ (ρ = density and v = local speed) is inserted for the body force in the subdomain settings. For shear flow along the cylinder direction, we used

COMSOL’s steady-state diffusion model. The speed in this case only has a single nontrivial component. The speed (or, more precisely, the momentum) obeys a diffusion equation, where the role of the diffusivity is taken by the kinematic viscosity, η/ρ . In order to recover oscillating shear waves, the term $-i\omega c$ (c is the concentration, equivalent to momentum) must be inserted for the reaction rate in the COMSOL subdomain settings.

Typical solutions of this model are vertical and horizontal components of flow velocities and pressure in the liquid surrounding the hemicylinders. They are shown in parts b, c, and d of Figure 4, respectively. The integrated tangential force onto the domain boundary at the top of the cell was calculated from the velocity fields, such as those shown in Figure 4 parts b and c, in the postprocessing mode. Division by the width of the cell yields the stress, σ . This stress is inserted into the small-load approximation (eq 3), which then leads to ΔF and $\Delta\Gamma$. The values of ΔF and $\Delta\Gamma$ displayed in Figure 5 parts a and b are differences in ΔF and $\Delta\Gamma$ between a crystal loaded with both a liquid and adsorbed vesicles and a crystal loaded with the liquid only. This involves taking a difference between two large numbers and imposes a rather stringent requirement on the accuracy of the model calculation. We show in ref 20 that these requirements are satisfied.

This model is not intended as a truly realistic representation of adsorbed particles. No attempt was made to make the agreement with experiments quantitative. This would be potentially misleading because it is entirely unclear whether an adsorbed vesicle or a virus particle may be presented as a hemisphere with a viscosity a few fold higher than that of water. The problem per se has so many free parameters that agreement between the model and the experimental data can be achieved with a diverse set of choices. We on purpose show results where the agreement is only qualitative (Figure 5).

Results

Representative sets of data for liposomes extruded through filters with pore sizes of 50 and 100 nm, respectively, adsorbing on titania, and ~30 nm CPMV particles adsorbing on gold, are shown in Figure 2. The actual sizes of liposomes and CPMV particles are listed in Table 1. In all three cases, the frequency decreases and the bandwidth increases as particles adsorb to the surface. The values of the two parameters saturate after some time at the so-called asymptotic shifts. In the case of liposomes, this behavior is known to correspond to intact liposome adsorption on the surface.^{31,32} The asymptotic

(30) Lin, T. W.; Chen, Z. G.; Usha, R.; Stauffacher, C. V.; Dai, J. B.; Schmidt, T.; Johnson, J. E. *Virology* **1999**, *265*(1), 20–34.

(31) Keller, C. A.; Kasemo, B. *Biophys. J.* **1998**, *75*, 1397–1402.

(32) Keller, C. A.; Glasmästar, K.; Zhdanov, V. P.; Kasemo, B. *Phys. Rev. Lett.* **2000**, *84*(23), 5443–5446.

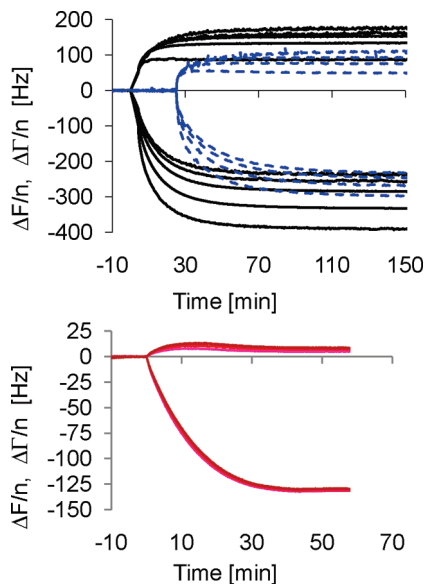


Figure 2. Typical QCM results of liposome and virus adsorption experiments. DPPC liposomes of two sizes adsorbing on titania (a) and CPMV particles adsorbing on gold (b) were used in this study. Bandwidth shifts are positive, frequency shifts are negative, both are scaled by the overtone order. (a) Black solid lines: 114 nm liposomes, extruded through 100 nm diameter filters. Blue dashed lines: 86 nm liposomes, extruded through 50 nm diameter filters. The two sets of curves in (a) are offset by 25 min along the time axis. Every second overtone is shown ($n = 3, 7, 11, 15$). (b) In the case of CPMV particles, the overtones nearly overlap, but the bandwidth shifts are sufficiently large for the behavior to be considered non-Sauerbrey. Overtones $n = 5$ (red), 9 (magenta), and 13 (brown) are shown, while $n = 3, 7$, and 11 are omitted for clarity. Note that the scales on the y-axes in (a) and (b) are quite different.

shifts are larger for larger objects, as reported previously.^{17,33} A value of ~ -135 Hz for the asymptotic frequency shift observed in the case of CPMV particles reproduces previous results obtained under identical conditions,²¹ and is only slightly higher than that reported for the adsorption of CPMV on streptavidin-coated supported lipid bilayers.²⁵

In the case of CPMV particles, the asymptotic shifts are similar on different overtones, from $n = 3$ –13. Bandwidth shifts are nevertheless nonzero: $\Delta\Gamma/n$ between 2.8 and 8.5 Hz on overtones $n = 3$ –13 was observed (this corresponds to dissipation shifts of 1.1 to 3.4×10^{-6} ; the larger values are observed on the higher-order overtones).

In the case of liposomes, the asymptotic shifts observed on different overtones are quite different; the behavior is distinctly non-Sauerbrey. Those obtained for the DPPC liposomes extruded through 50 nm pore diameter filters are somewhat smaller than those reported by us previously.¹⁷ There are no values in the literature for DPPC liposomes extruded through the 100 nm pore diameter filters, but the results obtained with DPPC liposomes can be compared with those obtained with various other phosphatidyl cholines containing unsaturated chains, such as dioleoyl or palmitoyl oleoyl (DOPC and POPC, respectively):^{17,33} invariably, the magnitude of the asymptotic shifts observed with the DPPC liposomes is larger than that observed with DOPC or POPC liposomes of similar size. This observation has been discussed in terms of the difference in the bending moduli between the

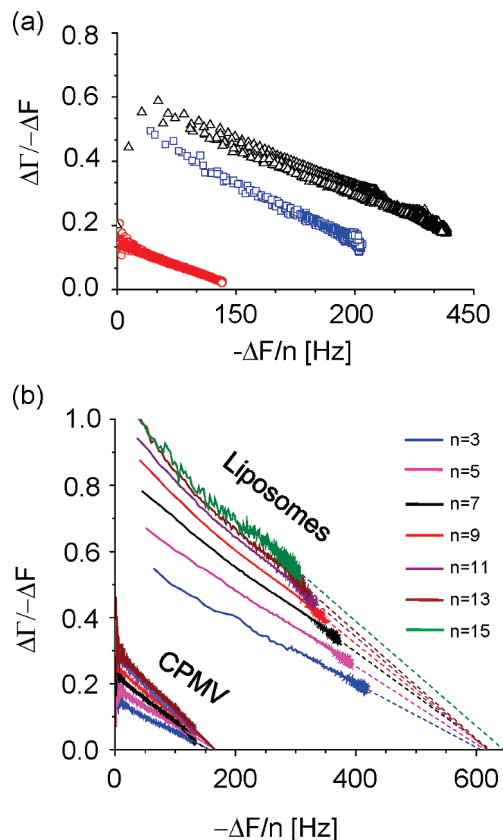


Figure 3. Dependence of the $\Delta\Gamma/-\Delta F$ ratio on the particle size and coverage. (a) The effect of surface coverage on the bandwidth shift to the frequency shift ratio, $\Delta\Gamma/-\Delta F$, can be separated from that of the particle size. Three curves are shown: black triangles, representing 114 nm liposomes; blue squares, representing 86 nm liposomes; and red circles, representing CPMV particles (~ 30 nm). Only the data for the third overtone are plotted. The ratio increases with the particle size but decreases with increasing magnitude of the frequency shift. Equation 2 predicts that the ratio increases slightly with the surface coverage; see Supporting Information. The plot of the $\Delta\Gamma/-\Delta F$ ratio vs the frequency shift indirectly examines the dependence of the ratio on the surface coverage (c.f. Figure 1), because the magnitude of the frequency shift increases with the surface coverage, even though the dependence of the frequency shift on the surface coverage is not linear.^{19–21} (b) Plotting the bandwidth shift to the frequency shift ratio, $\Delta\Gamma/-\Delta F$, as a function of the scaled frequency shift for several overtones, reveals a common intercept with the $-\Delta F/n$ axis. Data for the 114 nm liposomes ($n = 3$ –15) and for CPMV particles ($n = 3, 7$ –13) are shown. Dashed lines are linear regression fits to the data. In the case of CPMV, the data from higher overtones overlap much more closely than in the case of liposomes (c.f. Figure 2). There is a pronounced nonlinearity in the $\Delta\Gamma/\Delta F$ vs $-\Delta F/n$ curves at small values of the frequency shift.

two lipids. The bilayer bending modulus of DPPC is $\sim 10^{-18}$ J,³⁴ while that of DOPC and POPC is $\sim 10^{-20}$ J.³⁵ Therefore, DPPC liposomes are not expected to deform upon adsorption as much as the softer DOPC or POPC ones,^{36,37} forming thicker layers.¹⁷

Instead of attempting to extract layer properties by fitting the data with the model based on eq 1, as has been done previously,^{10,14–18} in this study we examine the behavior of

(34) Lee, C. H.; Lin, W. C.; Wang, J. P. *Phys. Rev. E* **2001**, 6402(2), art-020901.

(35) Rawicz, W.; Olbrich, K. C.; McIntosh, T.; Needham, D.; Evans, E. *Biophys. J.* **2000**, 79(1), 328–339.

(36) Seifert, U. *Adv. Phys.* **1997**, 46(1), 13–137.

(37) Seifert, U.; Lipowsky, R. *Phys. Rev. A* **1990**, 42(8), 4768–4771.

(33) Reimhult, E.; Hook, F.; Kasemo, B. *J. Chem. Phys.* **2002**, 117(16), 7401–7404.

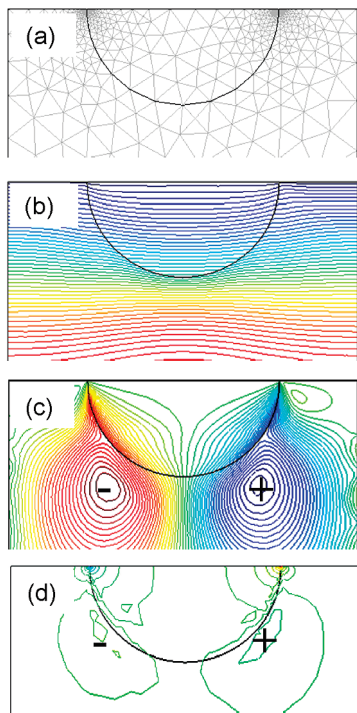


Figure 4. Typical solution of the FEM model: (a) geometry and mesh, (b) vertical component of the speed of flow, (c) horizontal component of the speed of flow, and (d) pressure. See text for details.

the bandwidth shift-to-frequency shift ratio, $\Delta\Gamma/\Delta F$ and compare it with the predictions of the model (eq 2). We do so by plotting the ratio versus the magnitude of the frequency shift in Figure 3. Contrary to the predictions of eq 2, the $\Delta\Gamma/\Delta F$ ratio decreases as a function of the magnitude of the frequency shift (Figure 3). To understand the origin of this discrepancy, we undertook FEM calculations for a comparable geometry to obtain the average stress at crystal–sample interface due to the flow of the surrounding liquid (Figure 4a). The average stress is then converted into frequency and bandwidth shifts using the small-load approximation (eq 3; see the Modeling section for details). The results of these calculations are shown in Figure 5. Panels (a) and (b) show the shifts in frequency (ΔF) and bandwidth ($\Delta\Gamma$) versus coverage. Both curves are nonlinear, and the ratio of the two strongly decreases with coverage (panel c). This decrease is of hydrodynamic origin.

We wish to note that FEM calculations are not meant to yield quantitative agreement with the experiment. Many features visible in Figure 5 are, in fact, different from those observed experimentally (Figure 3). Such an agreement could have been achieved by suitably adapting the parameters of the model. However, there would have been a number of different ways to reach such an agreement, and the results might be easily overinterpreted. The purpose of the calculation is only to show that accounting for hydrodynamic effects at the heterogeneous interface reproduces the decrease of the $\Delta\Gamma/\Delta F$ ratio with coverage.

Experimentally, the decrease of the $\Delta\Gamma/\Delta F$ ratio with $-\Delta F/n$ is observed to be linear over a large range of frequency shifts (Figure 3). The linear portions of the $\Delta\Gamma/\Delta F$ ratio versus $-\Delta F/n$ curves obtained at different overtones extrapolate to a frequency-independent intercept with the $-\Delta F/n$ axis (Figure 3b). Such a n -independent value of $-\Delta F/n$ at a

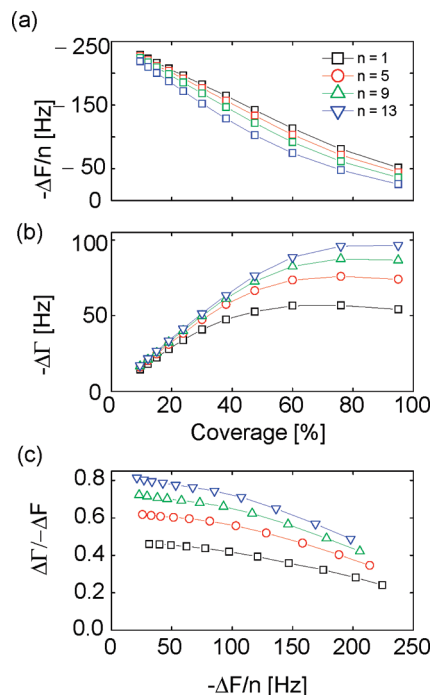


Figure 5. Results from FEM calculations: (a), (b) frequency shift, ΔF , and bandwidth shift, $\Delta\Gamma$, versus coverage; (c), (d) $(\Delta\Gamma/\Delta F)$ versus normalized frequency shift ($-\Delta F/n$). The ratio decreases with increasing coverage because hydrodynamic dissipation is more prominent at low coverage.

zero $\Delta\Gamma/\Delta F$ ratio by definition corresponds to a Sauerbrey mass.⁶ We will refer to this as the extrapolated Sauerbrey mass or thickness. In Table 1, this extrapolated Sauerbrey mass and the corresponding thickness are compared with the expectations that are based on the liposome diameter as measured by dynamic light scattering and the spherically averaged diameter of the virus particle. There is a clear correlation between the size of the particles in solution and the extrapolated Sauerbrey thickness. Overtones $n = 17$ and $n = 19$ had to be excluded from this analysis in most of the experiments, because the value of the intercept for these two overtones often deviated significantly from the rest (not shown). Although these overtones were also often much more noisy than the lower overtones, this could be an interesting frequency-dependent effect that we are unable to discern for the moment.

Liposome sizes, used in the comparison described above, deserve a comment. Complications with determining the exact size (distributions) of liposome suspensions from dynamic light scattering measurements are well-known; in particular, the Z -averaged size, obtained with the so-called second-order cumulant analysis of dynamic light scattering data, is weighted toward the larger sizes.³⁸ This problem complicates a further quantitative comparison between the liposome diameter in solution and the extrapolated Sauerbrey thickness.

Discussion

The central result of this work is the demonstration that the behavior of heterogeneous films—films composed of

(38) Schurtenberger, P.; Newman, M. E. Characterization of biological and environmental particles using static and dynamic light scattering. In *Environmental Particles*; Buffle, J., vanLeeuwen, H. P., Eds.; Lewis Publishers: Boca Raton, FL, 1993; Vol. 2, pp 36–115.

individual objects, such as those shown in Figure 1—in the QCM differs from the predictions of the effective media approximation exemplified by eq 1. The difference is well-illustrated by examining the behavior of the $\Delta\Gamma/-\Delta F$ ratio (Figure 3), which increases with object size (d , Figure 1) but decreases with the coverage (θ , Figure 1). In the case of homogeneous films, the $\Delta\Gamma/-\Delta F$ ratio should either be independent of acoustic thickness (h , Figure 1) or increase with it, while both object size and surface coverage affect the acoustic thickness in the same way. The former situation is valid for very thin films, while the latter holds for thicker films; see eq 2. Recent experimental observations reported by Tsortos et al. with DNA films are consistent with these predictions.¹³ Similarly, in the Supporting Information, we present an example of an increasing $\Delta\Gamma/-\Delta F$ ratio for a polymer film. Therefore, plots such as those shown in Figure 3 can be used to test whether or not a film can be treated as acoustically homogeneous.

In order to reconcile the behavior that we observe in the case of a heterogeneous film with the model based on homogeneous films, one is forced to introduce a coverage-dependent compliance $J^*(\theta)$ that decreases with increasing coverage (the film stiffens with increasing coverage). This is what has effectively been done in the previous studies.^{10,14–18} Proposing such coverage-dependent film stiffening amounts to postulating a long-range interaction between the adsorbed particles. An example of such a long-range interaction is that caused by the disruption of the flow of liquid in the vicinity of the surface by the adsorbed species. This hydrodynamic effect is taken into account in the FEM calculations (Figures 4 and 5). The results of the FEM calculations qualitatively reproduce the observed decrease of the $\Delta\Gamma/-\Delta F$ ratio with the surface coverage. Therefore, fitting QCM data obtained on heterogeneous films with the model based on homogeneous films amounts to assigning to the film effective elastic constants that contain a hydrodynamic contribution. We have recently presented a similar conclusion in two other studies focused on protein adsorption.^{19,20} One of these relied on the FEM calculations.²⁰

The picture of QCM response from heterogeneous films that emerges from this and our previous studies²⁰ is the following. In the case of heterogeneous films, there are essentially two channels of energy dissipation: that in the adsorbed particles themselves and that in the liquid surrounding the particles. The extent of the two contributions will determine the shape of the $\Delta\Gamma/-\Delta F$ versus $-\Delta F/n$ plot.

The first channel contributes a certain amount of energy dissipated per particle, which remains about constant throughout the adsorption process, at least until the particles begin to interact with each other. In the case of sufficiently stiff particles, this channel may be negligible. That is to say, a homogeneous film of the same material would behave as a Sauerbrey film, exhibiting negligible bandwidth shifts and overtone dispersion. This analysis is based directly on the behavior of homogeneous films, which is well-understood in the framework of the effective media approximation (eq 1).

The amount of energy dissipated in the liquid—the second channel—diminishes with increasing surface coverage. To understand why this occurs, consider that the $\Delta\Gamma$ in the $\Delta\Gamma/-\Delta F$ term is the difference in energy dissipation between the crystal with the adsorbed film and the bare crystal. The latter is essentially smooth, presenting a homogeneous surface to the surrounding liquid. The adsorbed film becomes more homogeneous as the surface coverage of the adsorbed

particles increases, which leads to the diminishing of the energy dissipated per adsorbed particle. Judging from the plots shown in Figure 3, this pathway of energy dissipation is the dominant one in the case of the adsorbed virus particles and liposomes used in this study. The extrapolation procedure used here to determine the geometrical height of the adsorbed objects (d , Figure 1) essentially yields the thickness of an equivalent homogeneous film. If energy dissipation in the particles themselves is negligible, this film will behave as a Sauerbrey film and the overtones will cross at the x -axis, where dissipation is zero. On the other hand, significant energy dissipation in the particles themselves will lead to overtone dispersion even in a homogeneous film, and the $\Delta\Gamma/-\Delta F$ versus $\Delta F/n$ plot will look different—more closely resembling that observed in the case of homogeneous films (see, for example, Figure S1 in Supporting Information). Very little can be said at this point as to why the $\Delta\Gamma/-\Delta F$ versus $\Delta F/n$ plot is linear.

The above line of argument is quite independent of the actual mechanism, by which energy in the liquid surrounding the particles is dissipated. However, the mechanism needs to be considered in light of the remarks made in the previous literature⁷ concerning the inability of theories dealing with rough/heterogeneous interfaces^{39–41} to account for the large bandwidth shifts observed experimentally in surface-adsorbed protein and liposome layers. In those previous works, the shear-induced motion of the adsorbed particles had not been considered. We pointed out in our recent work²⁰ that even very stiff/strongly attached particles will move under shear relative to the crystal surface; softer particles will do so to an even greater extent. This provides the additional mechanism for energy dissipation in the liquid surrounding the adsorbed particles. Its details are still being worked out and will be presented in a separate publication. We wish to once more stress the following point: the statement that energy dissipation in the liquid dominates over that in the particles is deduced from the experiment (Figure 3) and does not depend on the particular details of the mechanism by which this occurs.

Conclusions

Many films studied with quartz crystal microbalance are heterogeneous in nature—in the sense that they are composed of discrete, isolated entities adsorbed or attached to the surface of the quartz crystal. In this study, we investigated the effect this heterogeneity has on the QCM response. We found that, because of the effects of the liquid surrounding the particles, these films behave in a qualitatively different way than their homogeneous counterparts. The differences in behavior are exemplified by the dependence of the ratio of bandwidth shift, $\Delta\Gamma$, to the negative of the frequency shift, $-\Delta F$, the so-called Df ratio, on the surface coverage and size of the particles. The ratio increased with particle size but decreased with surface coverage, contrary to the expectation based on the behavior of homogeneous films that this ratio is either independent of film thickness or increases with it. This demonstrates that films composed of individual entities—heterogeneous films—cannot be adequately treated within the context of the effective media approximation, as has been done until now. Analysis of the $\Delta\Gamma/-\Delta F$

(39) Urbakh, M.; Daikhin, L. *Langmuir* **1994**, *10*(8), 2836–2841.

(40) Urbakh, M.; Daikhin, L. *Phys. Rev. B* **1994**, *49*(7), 4866–4870.

(41) Daikhin, L.; Urbakh, M. *Langmuir* **1996**, *12*(26), 6354–6360.

versus $-\Delta F/n$ plots may allow films that can be treated as homogeneous to be distinguished from those that may not. Interestingly, these plots revealed an extended linear range, which could be extrapolated to the intercept with the x -axis. This intercept was common for different overtones and could be used to define a thickness. This extrapolated thickness was found to correlate with the diameter of adsorbing particles in solution.

Acknowledgment. I.R. and R.R. gratefully acknowledge funding from the Department of Industry of the Basque Government. Funding was also provided from the American Heart Association Postdoctoral Fellowship to N.F.S. Dr. M. Manchester is thanked for providing resources and facilities for production of CPMV. The authors would like to thank Johanna Bünsow (TU Clausthal) for providing the data from the study presented in ref 42 described in the Supporting Information and Joseba Irigoyen (CIC biomaGUNE) for assistance with constructing the homemade QCM instrument.

Appendix

Here, we present the derivation of the equation for the $\Delta\Gamma/-\Delta F$ ratio, eq 2. In the limit of the small-load approximation,⁵ the frequency shift of a quartz crystal due to a homogeneous, viscoelastic film in liquid is given by

$$\frac{\Delta F^*}{f_F} = \frac{i}{\pi Z_q} \left(i Z_f \frac{Z_f \tan(k_f h_f) - i Z_{\text{liq}}}{Z_f + i Z_{\text{liq}} \tan(k_f h_f)} - Z_{\text{liq}} \right) \quad (\text{A1})$$

where ΔF^* is the complex frequency shift ($\Delta F^* = \Delta F + i\Delta\Gamma$), f_F is the frequency of the fundamental, Z_f , Z_{liq} , and Z_q are the acoustic impedances of the film, the liquid, and the AT-cut quartz, respectively, k_f is a wave vector, and h_f is the acoustic thickness of the film.

Wave vector k_f is defined as $k_f = \omega/c_f$ with the speed of shear acoustic sound waves in the film c_f and $\omega = 2\pi f$. Multiplying both sides by the acoustic thickness and using the relations $m_f = \rho_f h_f$ and $Z_f = \rho_f c_f$, where m_f is the mass of the film and ρ is its density, one obtains the following:

$$k_f h_f = \frac{\omega}{c_f} h_f = \frac{\omega}{\rho_f c_f} \rho_f h_f = \frac{\omega}{Z_f} m_f \quad (\text{A2})$$

Inserting eq A2 into eq A1 and rearranging, one obtains for the frequency shift

$$\frac{(\Delta F + i\Delta\Gamma) \pi Z_q}{f_F} = -Z_f \frac{Z_f \tan\left(\frac{\omega m_f}{Z_f}\right) - i Z_{\text{liq}}}{Z_f + i Z_{\text{liq}} \tan\left(\frac{\omega m_f}{Z_f}\right)} - i Z_{\text{liq}} \quad (\text{A3})$$

(42) Reuber, J.; Reinhardt, H.; Johannsmann, D. *Langmuir* **2006**, *22*(7), 3362–3367.

The term on the right-hand side is expanded up to a second order in m_f to obtain

$$\begin{aligned} \frac{(\Delta F + i\Delta\Gamma) \pi Z_q}{f_F} &= -\omega m_f \left(1 - \frac{Z_{\text{liq}}^2}{Z_f^2} \right) + \\ \frac{i\omega^2 m_f^2 Z_{\text{liq}}}{Z_f^2} \left(1 - \frac{Z_{\text{liq}}^2}{Z_f^2} \right) &= -\omega m_f \left(1 - \frac{Z_{\text{liq}}^2}{Z_f^2} \right) \left(1 - i \frac{\omega m_f Z_{\text{liq}}}{Z_f^2} \right) \end{aligned} \quad (\text{A4})$$

$$\frac{\Delta\Gamma}{-\Delta F} = \frac{-\text{Im} \left\{ \left(1 - \frac{Z_{\text{liq}}^2}{Z_f^2} \right) \left(1 - i \frac{\omega m_f Z_{\text{liq}}}{Z_f^2} \right) \right\}}{\text{Re} \left\{ \left(1 - \frac{Z_{\text{liq}}^2}{Z_f^2} \right) \left(1 - i \frac{\omega m_f Z_{\text{liq}}}{Z_f^2} \right) \right\}} \quad (\text{A5})$$

When taking the ratio of the imaginary and real parts of eq A5, we make the further assumption that the liquid is much softer than the film. Accordingly, the second terms in the brackets are $\ll 1$. The real part of the terms in brackets then is of order 1 in both cases. The denominator turns to unity, and the $\Delta\Gamma/-\Delta F$ ratio is equal to the imaginary part of the terms in brackets. Further, since the second terms in the brackets are both much smaller than the first terms, one may neglect the product of the two. These approximations yield the following:

$$\begin{aligned} \frac{\Delta\Gamma}{-\Delta F} &\approx -\text{Im} \left(1 - \frac{Z_{\text{liq}}^2}{Z_f^2} - i \frac{\omega m_f Z_{\text{liq}}}{Z_f^2} \right) = \\ &\text{Im} \left(\frac{Z_{\text{liq}}^2}{Z_f^2} + i \frac{\omega m_f Z_{\text{liq}}}{Z_f^2} \right) \end{aligned} \quad (\text{A6})$$

Inserting $Z_{\text{liq}} = \sqrt{i\omega\rho_{\text{liq}}\eta_{\text{liq}}}$ and $1/Z_f^2 = J_f/\rho_f$ leads to the following expression for the bandwidth shift to the frequency shift ratio:

$$\frac{\Delta\Gamma}{-\Delta F} \approx \eta\omega J_f' \frac{\rho_{\text{liq}}}{\rho_f} + \omega h_f \sqrt{\frac{\rho_{\text{liq}}\omega\eta_{\text{liq}}}{2}} (J_f' + J_f'') \quad (\text{A7})$$

In the limit of $\rho_{\text{liq}} \approx \rho_f$, substituting $\omega = 2\pi f$ and rearranging eq A7 gives eq 2.

Supporting Information Available: The behavior of the $\Delta\Gamma/-\Delta F$ ratio in the case of a polymer gel—essentially a homogeneous film—forming in situ at the surface of the QCM crystal is presented in the Supporting Information. This material is available free of charge via the Internet at <http://pubs.acs.org>.